



**Ambient noise seismic imaging**

Journal:	<i>McGraw Hill 2008 Yearbook of Science &amp; Technology</i>
Manuscript ID:	YB09-0130
Manuscript Type:	Yearbook Article
Date Submitted by the Author:	23-Jun-2008
Complete List of Authors:	Ritzwoller, Michael
Keywords:	ambient noise, seismology, seismic tomography, Rayleigh wave, Love wave, surface wave
Abstract:	A recent innovation in seismic imaging based on using long time sequences of ambient seismic noise moves beyond some of the limitations imposed on earthquake-based methods to reveal higher resolution information about the crust and uppermost mantle. This method is called Ambient Noise Tomography (ANT), and has been applied predominantly to seismic surface waves. With the application of ANT to data from ambitious new deployments of seismic arrays, such as the EarthScope USArray in the United States, improved seismic models of the earth's crust and uppermost mantle at unprecedented resolution are rapidly emerging.



## Ambient Noise Seismic Imaging

*Michael H. Ritzwoller*

*Center for Imaging the Earth's Interior*

*Department of Physics*

*University of Colorado at Boulder*

*Boulder, CO 80309-0390 USA*

*Phone (303) 492 7075*

*Email: michael.ritzwoller@colorado.edu*

### Introduction

Traditional seismic imaging of large-scale structures within Earth's interior is based on observations of surface displacements following earthquakes or human-caused explosions. These methods measure body and surface wave travel times as well as whole waveforms typically following earthquakes, because of the expense and environmental impact of explosive sources. Such measurements are unraveled (inverted) to reveal the isotropic and anisotropic variation of compressional ( $V_p$ ) and shear ( $V_s$ ) wave speeds in Earth's crust, mantle, and core that are then interpreted in terms of temperature, composition, and fluid content. The ability of earthquake-based methods to resolve structural features within the Earth degrades during the propagation of the wave over long (teleseismic) distances. For seismic surface waves (Rayleigh and Love waves), teleseismic transmission results in the loss of the high frequencies needed to infer information about Earth's crust and uppermost mantle. A recent innovation in seismic imaging based on using long time sequences of ambient seismic noise moves beyond some of the limitations imposed on earthquake-based methods to reveal higher resolution information about the crust and uppermost mantle. This method is called Ambient Noise Tomography (ANT), and has been applied predominantly to seismic surface waves. With the application of ANT to data from ambitious new deployments of seismic arrays, such as the EarthScope USArray in the United States, improved seismic models of the earth's crust and uppermost mantle at unprecedented resolution are rapidly emerging.

### The idea of ambient noise tomography

Between earthquakes, seismometers continuously record surface displacements with a wide range of causes; e.g., wind, atmospheric pressure variations, fluid flows beneath and on the surface, human and animal motions, and ocean waves. Seismic waves produced by ocean waves, called microseisms, are particularly well studied and are observed to propagate deep into continental interiors. Microseismic amplitudes peak near 8 sec and 16 sec period, but extend to longer periods merging into the somewhat more enigmatic, but increasingly well studied, “earth hum” at periods above 20 sec. Debate continues into whether earth hum is generated predominantly in shallow waters like microseisms, or in deep waters. Recent evidence presented by B. Romanowicz and collaborators and others indicates that it is predominantly a shallow water phenomenon, but this does not preclude a deep water component.

Any mechanism that produces waves that propagate coherently between a pair of seismometers can be used as a basis for seismic tomography. This idea has a long history in seismology, but was resurrected by R. Weaver and O. Lobkis and other researchers in a series of papers beginning in 2001 that showed in the laboratory and theoretically that cross-correlations between recordings of diffuse waves at two receiver locations yield the “Green’s function” between these positions. The Green’s function is a seismic waveform that contains all of the information about wave propagation in the medium between the two stations. Once estimated, traditional seismic methods of tomography then can be applied to the Green’s function to recover information about the medium of transport.

The relevance of these results to large-scale earth imaging was not immediately clear, because the Earth’s ambient noise field, containing as it does energetic microseismic energy, is not diffuse, is probably not homogeneously distributed in azimuth, and its frequency content was poorly understood. In 2004, N. Shapiro and M. Campillo showed that coherent Rayleigh surface waves can be extracted from the Earth’s ambient noise field and that the primary frequency content of the waves lies in the microseismic and earth hum bands from about 6 sec to 100 sec period with the highest amplitudes in the microseismic band. Subsequent studies have confirmed that the full Green’s function does not emerge from cross-correlating seismic data because the cross-correlations are

1  
2  
3 dominantly surface waves, with Love waves also being observable. Nevertheless, the  
4 ability to constrain surface wave speeds at periods from 6 to 20 sec, which are sensitive  
5 to crustal depths but difficult to measure from teleseismic earthquakes, provided much of  
6 the early interest in the method.  
7  
8  
9

### 10 11 **Observations of broad-band surface waves** 12

13  
14 Seismic surface waves, in contrast with body waves, are waves that propagate in a  
15 waveguide near Earth's surface. The depth extent of the waveguide depends on  
16 wavelength; with a fair approximation being about a third of a wavelength. Thus, surface  
17 waves with periods below about 20 sec are sensitive to the crust and waves between 20  
18 and 100 sec period are sensitive predominantly to the uppermost mantle to a depth of  
19 about 150 km. Both Rayleigh (vertically polarized waves) and Love (horizontally  
20 polarized waves transverse to the direction of motion) waves are dispersive; their speeds  
21 depend on frequency with lower frequencies typically traveling faster than higher  
22 frequencies.  
23  
24  
25  
26  
27  
28  
29

30  
31 Surface waves appear strongly on cross-correlations of ambient noise and their dispersion  
32 characteristics are readily identifiable (Figure 1). G. Bensen and collaborators presented a  
33 primer on ambient noise data processing in 2007. They provide methods for removing  
34 earthquakes and instrumental irregularities from seismograms prior to cross-correlation  
35 and show that longer time series (a year or more) homogenize the azimuthal content of  
36 ambient noise, that reliable measurements require a station separation of at least two  
37 wavelengths, and that uncertainties can be estimated from the temporal repeatability of  
38 the measurements.  
39  
40  
41  
42  
43  
44

45  
46 The production of maps of the speed of Rayleigh or Love waves as a function of  
47 frequency is called surface wave tomography. What has come to be known as ambient  
48 wave tomography (ANT) is the generation of such maps from inter-station ambient noise  
49 cross-correlations. The first ambient noise tomographic images of Rayleigh wave group  
50 speeds in the microseismic band were presented simultaneously by N. Shapiro and  
51 collaborators and K. Sabra and collaborators in 2005 based on one to several months of  
52 data from stations in southern California. These studies were followed by a multiplicity  
53  
54  
55  
56  
57  
58  
59  
60

1  
2  
3 of applications around the world including studies in Europe, New Zealand, South Africa,  
4 Korea, Japan, Iceland, Canada, Australia, and China in addition to the US. Both Rayleigh  
5 and Love wave dispersion maps are now commonly obtained at periods from 6 sec to 100  
6 sec with the spatial extent of the study ranging up to the continental scale and time series  
7 lengths of more than 4 years used in some cases. ANT is most powerfully applied to large  
8 deployments of seismometers, such as the Transportable Array (TA) component of  
9 EarthScope/USArray (Figure 2), which includes more than 400 broad-band seismometers  
10 deployed concurrently with a station separation of about 70 km and is presently sweeping  
11 across the US. F. Lin and collaborators show that the resolution of ANT applied to  
12 EarthScope TA data is better than the inter-station spacing, which is unprecedented over  
13 an area the size of the western US. The construction of similar large-scale deployments of  
14 seismometers is occurring or planned in China and Europe.

15  
16  
17  
18  
19  
20  
21  
22  
23  
24  
25  
26  
27  
28  
29  
30  
31  
32  
33  
34  
35  
36  
37  
38  
39  
40  
41  
42  
43  
44  
45  
46  
47  
48  
49  
50  
51  
52  
53  
54  
55  
56  
57  
58  
59  
60  
There has remained pockets of concern among seismologists that ambient noise in the  
Earth does not meet the theoretical conditions on which ANT rests. In particular, the  
worry has been that the azimuthal inhomogeneity of ambient noise may, at worst, vitiate  
the method and, at best, generate biased measurements. Studies of the directionality of  
ambient noise published in 2006 and 2008 by L. Stehly and Y. Yang and their respective  
collaborators demonstrate that with the use of time series of a year or more in length,  
ambient noise propagates across a wide range of azimuths although there maybe some  
preferred directions. Simulations of the observed azimuthal content of ambient noise  
establish that measurement bias is small relative to other sources of measurement error.

### **3D images of Earth's interior**

The purpose of ANT is not just to reveal the speed of surface waves at different periods  
(Figure 2), but to use this information to unveil the three-dimensional (3-D) variation of  
seismic waves in Earth's interior in order to advance knowledge of temperature,  
composition, and fluid content which hold the key to the understanding of Earth  
processes. Recent studies, such as that by Y. Yang and collaborators in 2008 for the  
western US, which inverted ambient noise and earthquake derived information  
simultaneously, are now providing 3-D images of the crust and uppermost mantle over  
large areas in unprecedented detail (Figure 3). ANT provides not only better lateral

1  
2  
3 resolution over traditional surface wave methods in regions with good station coverage,  
4 but its broad frequency content, which extends to periods below 10 sec, also gives the  
5 vertical resolution needed to resolve crustal from mantle structures clearly.  
6  
7  
8  
9

### 10 11 12 **Applications other than earth imaging**

13  
14 Ambient noise can be exploited constructively in other contexts than Earth imaging.  
15 Other bodies in the solar system, for example, have been targets for the method. T.  
16 Duvall and collaborators in 1993 established time-distance seismology on the Sun  
17 (helioseismology) based on cross-correlating intensity fluctuations observed on the solar  
18 surface. In 2005, E. Larose and collaborators correlated seismic noise on the Moon's  
19 surface taken from the Apollo 17 Lunar Seismic Profiling Experiment, estimated  
20 Rayleigh wave group speeds between frequencies of 4 and 11 Hz, and inverted them to  
21 provide new information about the lunar regolith. They also established that the Sun  
22 actively generates the lunar seismic noise because of strong thermal gradients induced  
23 during the lunar day. These results suggest the extension of ambient noise tomography to  
24 planetary exploration where the origin of the noise may be quite different than on Earth.  
25 Back on Earth, variations in cross-correlations between stations can provide information  
26 about the changing state of the shallow crust that may, for example, precede volcanic  
27 activity or possibly earthquakes. In 2008, for example, F. Brenguier and collaborators  
28 showed how seismic wave speeds determined from ambient noise decreased before  
29 eruptions of the Piton de Fournaise volcano, presumably attributable to pre-eruptive  
30 inflation caused by increased magma pressure.  
31  
32  
33  
34  
35  
36  
37  
38  
39  
40  
41  
42  
43  
44  
45  
46  
47  
48  
49  
50

### 51 **Bibliography**

52  
53 Bensen, G.D., M.H. Ritzwoller, M.P. Barmin, A.L. Levshin, F. Lin, M.P. Moschetti,  
54 N.M. Shapiro, and Y. Yang, Processing seismic ambient noise data to obtain reliable  
55 broad-band surface wave dispersion measurements, *Geophys. J. Int.*, 169, 1239-1260,  
56 doi: 10.1111/j.1365-246X.2007.03374.x, (2007).  
57  
58  
59  
60

1  
2  
3  
4  
5  
6  
7  
8  
9  
10  
11  
12  
13  
14  
15  
16  
17  
18  
19  
20  
21  
22  
23  
24  
25  
26  
27  
28  
29  
30  
31  
32  
33  
34  
35  
36  
37  
38  
39  
40  
41  
42  
43  
44  
45  
46  
47  
48  
49  
50  
51  
52  
53  
54  
55  
56  
57  
58  
59  
60

Larose, E., A. Khan, Y. Nakamura, and M. Campillo, Lunar subsurface investigated from correlation of seismic noise, *Geophys. Res. Letts.*, 32, L16201, doi:10.1029/2005GL023518, (2005).

Lobkis, O.I. and R.L. Weaver, On the emergence of the Green's function in the correlations of a diffuse field, *J. Acoust. Soc. Am.*, 110(6), 3011-3017, (2001).

Shapiro, N.M. and M. Campillo, Emergence of broadband Rayleigh waves from correlations of the ambient seismic noise, *Geophys. Res. Lett.* 31, L07614, doi:10.1029/2004GL019491, (2004).

Shapiro, N.M. M. Campillo, L. Stehly, and M.H. Ritzwoller, High resolution surface wave tomography from ambient seismic noise, *Science*, 307(5715), 1615-1618, 11 March (2005).

Yang, Y., M.H. Ritzwoller, F.-C. Lin, M.P. Moschetti, and N.M. Shapiro, The structure of the crust and uppermost mantle beneath the western US revealed by ambient noise and earthquake tomography, submitted to *J. Geophys. Res.*, (2008).

#### **Additional Readings (other studies referred to in the text)**

Brenguier, F., N.M. Shapiro, M. Campillo, V. Ferrazzini, Z. Duputel, O. Coutant, and A. Nercessian, Towards forecasting volcanic eruptions using seismic noise, *Nature Geoscience*, doi:10.1038/ngeo104, 20 January (2008).

Lin, F., M.P. Moschetti, and M.H. Ritzwoller, Surface wave tomography of the western United States from ambient seismic noise: Rayleigh and Love wave phase velocity maps, *Geophys. J. Int.*, doi:10.1111/j1365-246X.2008.03720.x, (2008).

Duvall, T.L., S.M. Jefferies, J.W. Harvey, and M. A. Pomerantz, Time-distance helioseismology, *Nature*, 362, 430-432, (1993).

Rhie, J. and B. Romanowicz, A study of the relation between ocean storms and the Earth's hum, *Geochem., Geophys., Geosys.*, 7(10), Q10004, doi:10.1029/2006GC001274, (2006).

Sabra, K.G., P. Gerstoft, P. Roux, and W.A. Kuperman, Surface wave tomography from microseisms in Southern California, *Geophys. Res. Letts.*, 32, L14311, doi:10.1029/2005GL023155, (2005).

Stehly, L., M. Campillo, and N. M. Shapiro, A study of the seismic noise from its long range correlation properties, *J. Geophys. Res.*, 111, B10306, doi:10.1029/2005JB004237, (2006).

Yang, Y. and M.H. Ritzwoller, The characteristics of ambient seismic noise as a source for surface wave tomography, *Geochem., Geophys., Geosys.*, 9(2), Q02008, 18 pages, doi:10.1029/2007GC001814, 2008.

1  
2  
3 McGraw-Hill articles: Coda wave interferometry, Seismology, Earth oscillations.  
4  
5

### 6 **Related Web Sites**

7  
8 EarthScope: <http://www.earthscope.org> or <http://www.iris.edu>  
9

10  
11 Ambient noise tomography in the US: [http://ciei.colorado.edu/ambient\\_noise](http://ciei.colorado.edu/ambient_noise)  
12  
13  
14  
15  
16  
17  
18

### 19 **Figure Captions**

20  
21  
22  
23  
24 **Figure 1.** Cross-correlation between two years of ambient noise recorded on the vertical  
25 components of two seismic stations in the western US. The stations are  
26 EarthScope/USArray Transportable Array stations M03 (McCloud, CA) and Y14A  
27 (Wickenburg, AZ) separated by a distance of 1144 km. Arrivals at positive and negative  
28 times are for waves traveling in opposite directions between the stations. Rayleigh waves  
29 arrive at times between 200 sec and 500 sec. (a) The broad-band cross-correlation is  
30 shown. (b) – (d) Band-pass filters are applied to the broad-band cross-correlation  
31 centered on 10 sec, 20 sec, and 50 sec period, respectively. The longer periods are seen to  
32 travel faster, indicative of the dispersive nature of the Rayleigh wave. (Figure courtesy of  
33 Morgan Moschetti.)  
34  
35  
36  
37  
38  
39  
40  
41  
42  
43  
44

45  
46 **Figure 2.** Rayleigh wave group speed map at 8 sec period across the western US  
47 determined by ambient noise tomography applied to more than two years of data from the  
48 EarthScope/USArray Transportable Array. Slow wave speeds are shown in white and  
49 faster speeds are indicated with darker shades of grey. Black lines delineate geological  
50 provinces. The 8 sec Rayleigh wave is sensitive to about the top 10 km of the crust  
51 beneath the surface. Slow speeds are associated with sedimentary basins (e.g., Central  
52 Valley in CA, Salton Trough in CA, Green River Basin in WY), deformed regions (e.g.,  
53  
54  
55  
56  
57  
58  
59  
60

1  
2  
3 CA coastal ranges, Olympic Peninsula in northwest WA; Yakima Fold Belt in central  
4 WA), and very hot areas (e.g., Yellowstone in WY). Faster regions are correlated with  
5 mountain belts (e.g., Sierra Nevada in CA; Cascade Range in CA, OR, WA; Peninsular  
6 Range in southern CA and Baja Mexico), massive flood basalts in OR and WA, and the  
7 Colorado Plateau near the Four-Corners region. (Figure courtesy of Morgan Moschetti.)  
8  
9  
10  
11  
12  
13  
14  
15

16 **Figure 3.** Images of the 3-D variation of shear wave speed ( $V_s$ ) in the crust and  
17 uppermost mantle determined from ambient noise and earthquake information. (a)  
18 Horizontal slice at 100 km depth. (b) Vertical profile underlying the white line in (a).  
19 Vertically exaggerated surface topography is presented at top and the black line indicates  
20 the Mohorovicic discontinuity, separating the crust from the mantle. In both panels,  $V_s$  is  
21 presented as the perturbation in percent from the average at each depth across the model.  
22 Numerous features are imaged in the crust and mantle. For example, in the mantle the  
23 subducting Juan de Fuca and Gorda plates are seen as high  $V_s$  beneath N. CA, OR, and  
24 WA in both (a) and (b). In (b), the high  $V_s$  subducting plate is overlain by low  $V_s$  speeds  
25 (high temperature and volatile content) beneath active volcanoes in the Cascade Range.  
26 (Figure courtesy of Yingjie Yang.)  
27  
28  
29  
30  
31  
32  
33  
34  
35  
36  
37  
38  
39  
40  
41  
42  
43  
44  
45  
46  
47  
48  
49  
50  
51  
52  
53  
54  
55  
56  
57  
58  
59  
60

1  
2  
3  
4  
5  
6  
7  
8  
9  
10  
11  
12  
13  
14  
15  
16  
17  
18  
19  
20  
21  
22  
23  
24  
25  
26  
27  
28  
29  
30  
31  
32  
33  
34  
35  
36  
37  
38  
39  
40  
41  
42  
43  
44  
45  
46  
47  
48  
49  
50  
51  
52  
53  
54  
55  
56  
57  
58  
59  
60

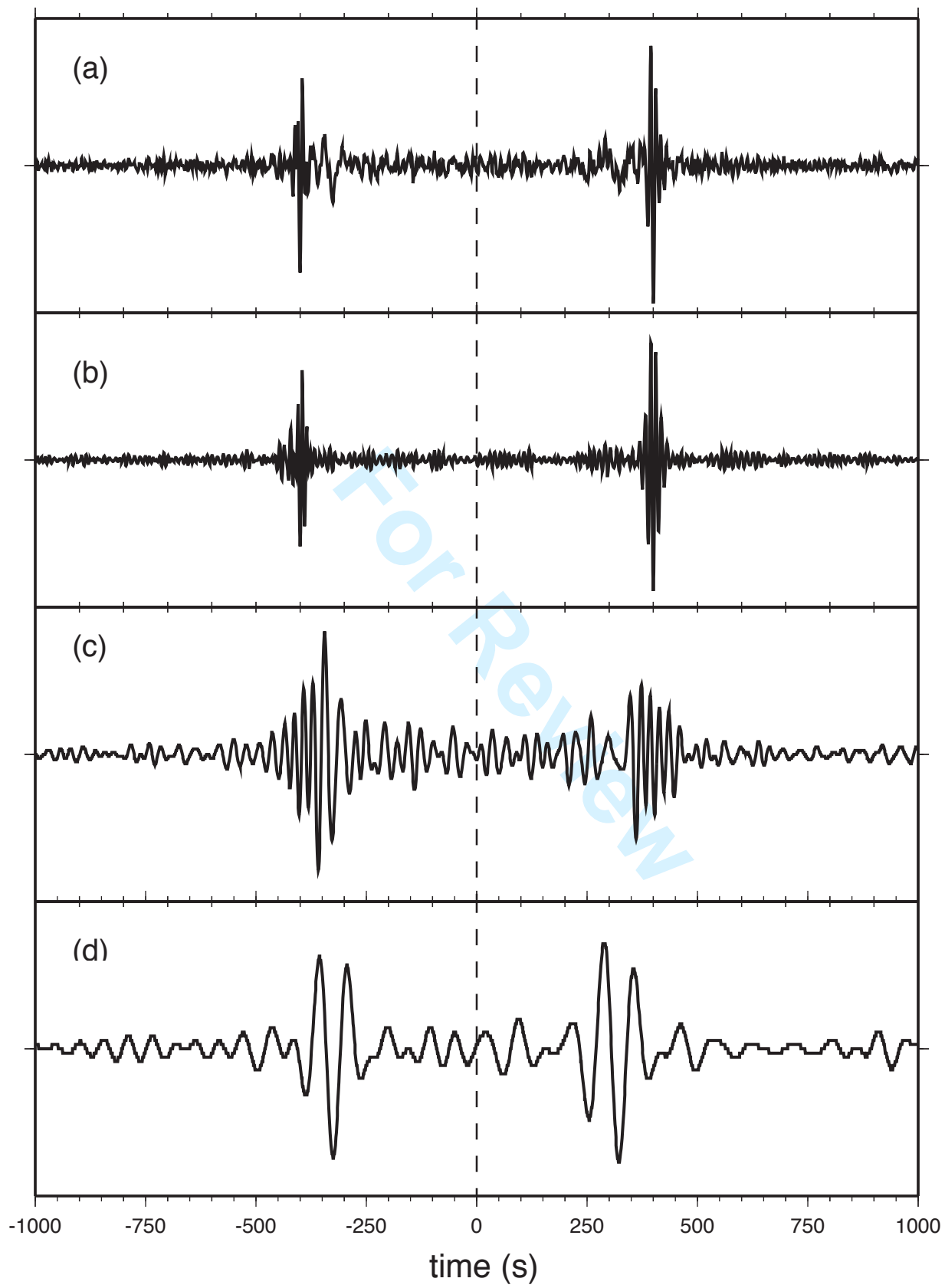


Figure 1

1  
2  
3  
4  
5  
6  
7  
8  
9  
10  
11  
12  
13  
14  
15  
16  
17  
18  
19  
20  
21  
22  
23  
24  
25  
26  
27  
28  
29  
30  
31  
32  
33  
34  
35  
36  
37  
38  
39  
40  
41  
42  
43  
44  
45  
46  
47  
48  
49  
50  
51  
52  
53  
54  
55  
56  
57  
58  
59  
60

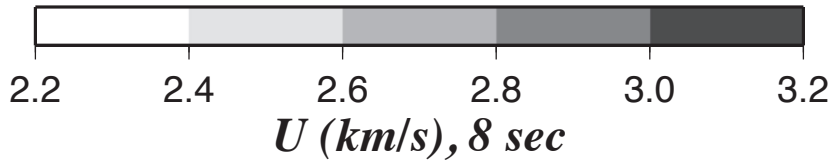
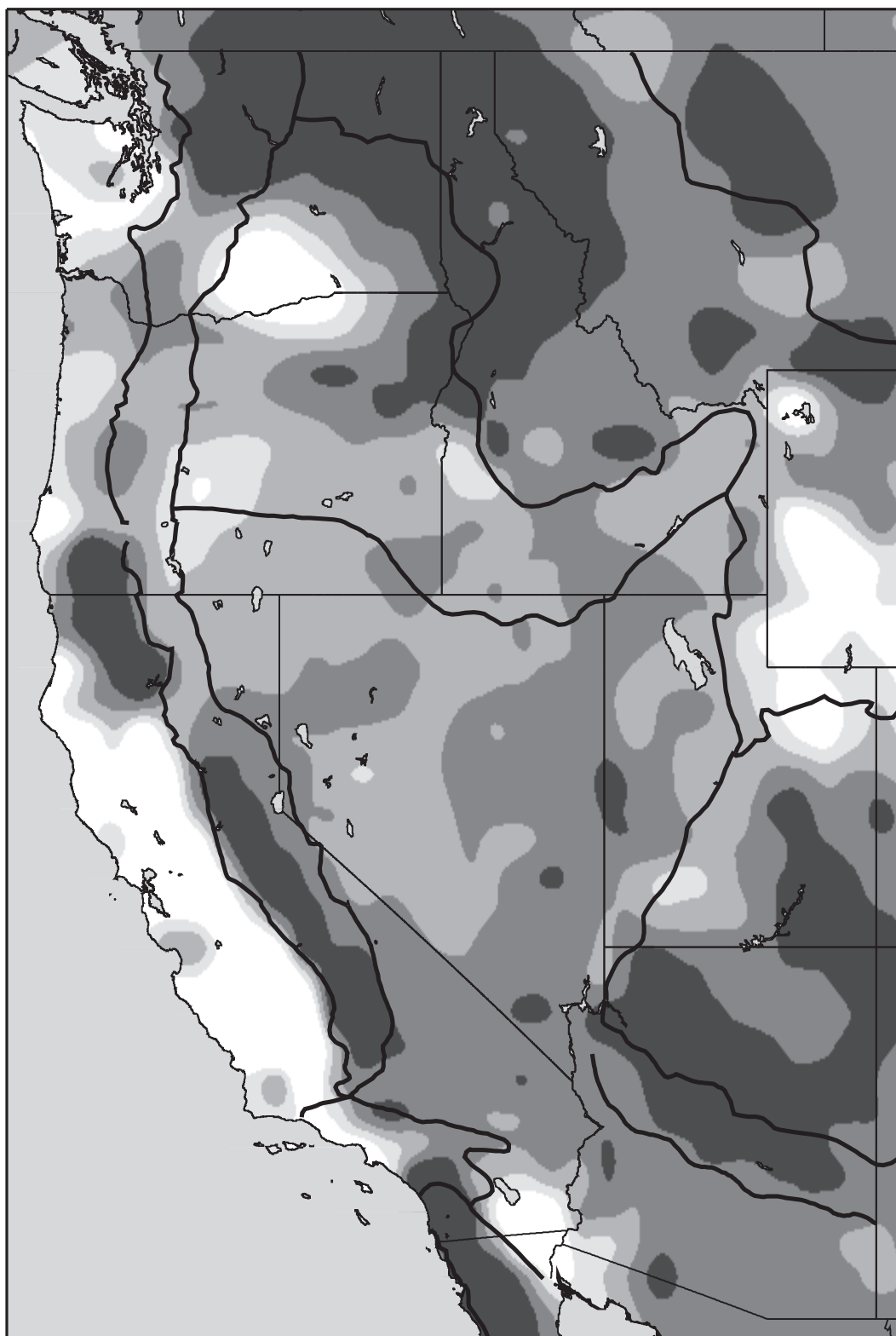


Figure 2 (black & white)

1  
2  
3  
4  
5  
6  
7  
8  
9  
10  
11  
12  
13  
14  
15  
16  
17  
18  
19  
20  
21  
22  
23  
24  
25  
26  
27  
28  
29  
30  
31  
32  
33  
34  
35  
36  
37  
38  
39  
40  
41  
42  
43  
44  
45  
46  
47  
48  
49  
50  
51  
52  
53  
54  
55  
56  
57  
58  
59  
60

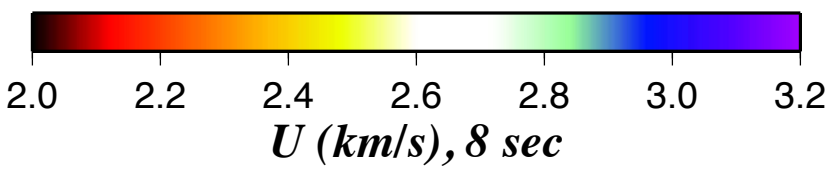
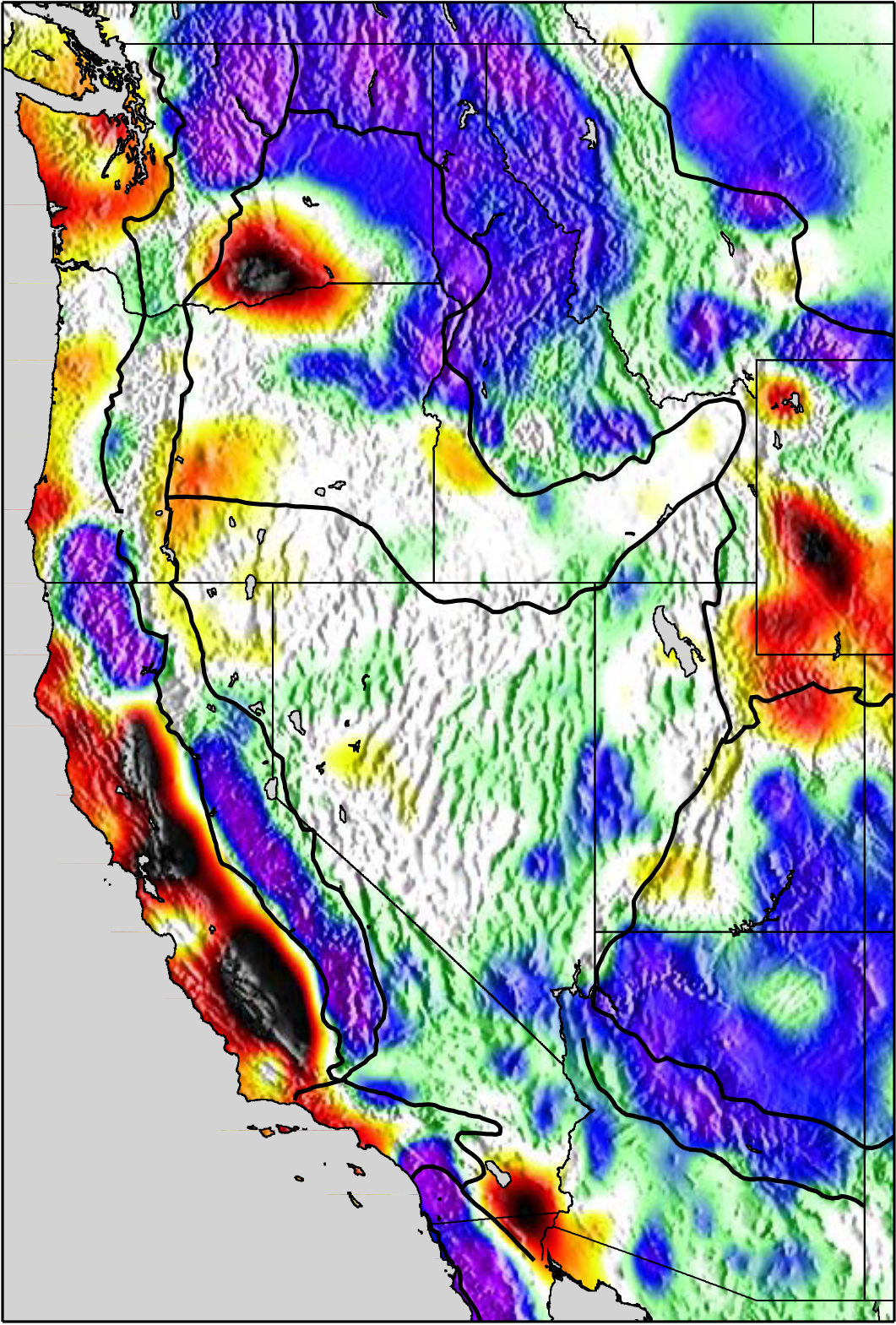
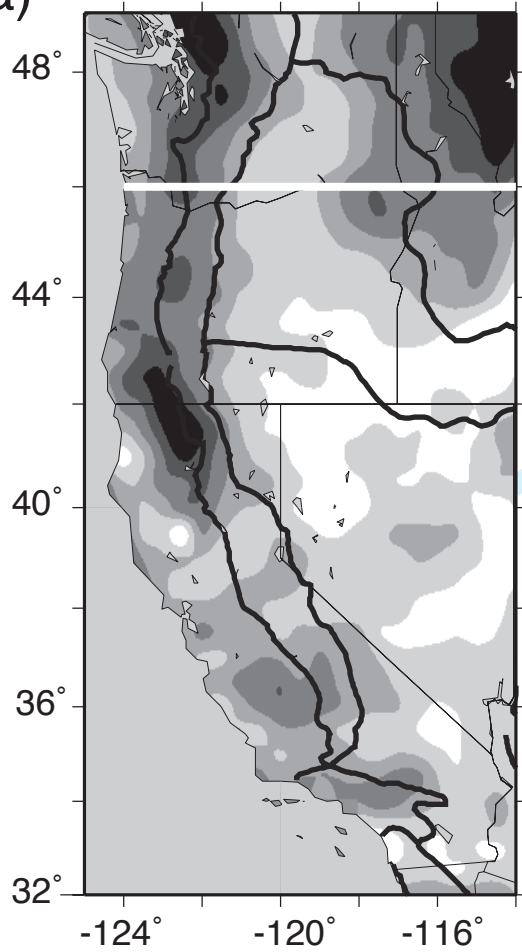


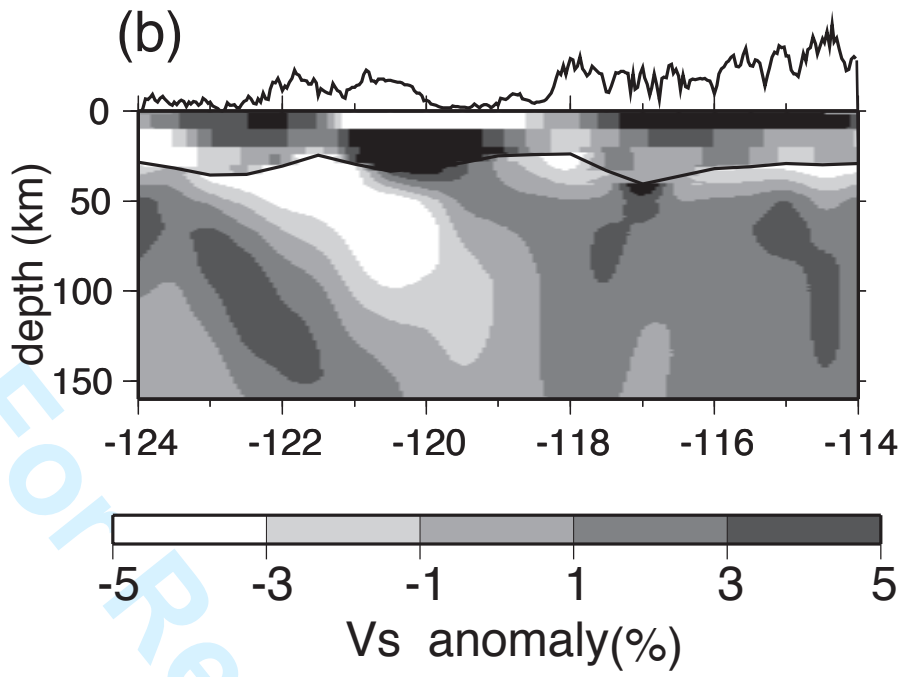
Figure 2 (color)

1  
2  
3  
4  
5  
6  
7  
8  
9  
10  
11  
12  
13  
14  
15  
16  
17  
18  
19  
20  
21  
22  
23  
24  
25  
26  
27  
28  
29  
30  
31  
32  
33  
34  
35  
36  
37  
38  
39  
40  
41  
42  
43  
44  
45  
46  
47  
48  
49  
50  
51  
52  
53  
54  
55  
56  
57  
58  
59  
60

(a)



(b)



For Review

1  
2  
3  
4  
5  
6  
7  
8  
9  
10  
11  
12  
13  
14  
15  
16  
17  
18  
19  
20  
21  
22  
23  
24  
25  
26  
27  
28  
29  
30  
31  
32  
33  
34  
35  
36  
37  
38  
39  
40  
41  
42  
43  
44  
45  
46  
47  
48  
49  
50  
51  
52  
53  
54  
55  
56  
57  
58  
59  
60

